Pergamon

PII: S0301-9322(96)00076-6

*Int. J. Multiphase Flow* Vol. 23, No. 2, pp. 377–395, 1997

0301-9322/97 $17.00 + 0.00

# NUMERICAL TREATMENT OF THE INSTABILITY AND THE BREAKUP OF A LIQUID CAPILLARY COLUMN IN A BOUNDED IMMISCIBLE PHASE

M. CHACHA, S. RADEV, L. TADRIST and R. OCCELLI

I.U.S.T.I.—U.M.R 169, U.P.—Centre de Saint Jérome, Case 162, Av. Escadrille Normandie Niemen, 13397 Marseille Cedex 20, France

*(Received 15 May 1995; in revised form 20 September 1996)*

**Abstract**—The capillary instability of an infinite axisymmetric viscous liquid column in an immiscible medium is investigated. The process of disintegration is simulated numerically using a (second-order) finite-difference method applied to the 'vorticity–stream function' formulation of the Navier–Stokes equations. These equations and corresponding boundary conditions are written in there detailed form including convective terms in Navier–Stokes equations and nonlinear terms in the mass and momentum conservation equations at the unknown interface. Then the evolution in time of a given cosinusoidal disturbance is studied subjected to the action of the nonlinear effects. In these conditions the formation of a satellite drop attached to the main drop is observed. In the case where the liquid column is submerged into a low density inviscid fluid, the basic characteristics of the column disintegration such as drops sizes and breakup time are in a good agreement with those calculated by previous authors. New results are obtained for the instability parameters of a liquid column surrounded by another viscous fluid. 

*Key Words:* jet in liquid–liquid systems, capillary instability, numerical simulation of jet disintegration, satellite formation

## 1. INTRODUCTION

In the recent years the capillary jets have been used in many practical applications such as printing, particle sorting, dispersing liquids, fibers spinning, etc. Most of these applications are based on the effects of jet instability, which gives rise to growing disturbances that finally break up the jet into drops.

Since 1878 when Rayleigh has published the first theoretical study of the stability of an inviscid liquid column into a nearly-zero-density inviscid fluid, the problem of capillary jet instability has been treated in numerous approaches. It is out of the scope of our paper to present a detailed review on the papers contributing to jet instability investigation. We focus mainly on some basic theoretical works, referencing for the others (including experimental papers) to several useful reviews. For the aims of the present paper it would be convenient to combine the previous works into two groups.

To the first group, we relate papers where the instability is studied for jets on which the surrounding fluid has no effect. As shown by Rayleigh the cylindrical column in such conditions is stable for all purely non-axisymmetric disturbances; however, in respect to axisymmetric disturbances it is stable or unstable, depending on whether the wavelength is less or greater than the circumference of the undisturbed cylinder. Many authors (see, e.g. the survey of McCarthy and Molloy 1974), among them, Weber (1931), studied the axi-symmetrical breakup of a liquid jet, including the effect of the viscosity.

To the second group those papers could be related in which at least some of the effects of the surrounding fluid is included in the analysis of the jet instability. The basic work in this group is the paper of Tomotika (1935) in which the relationship between the growth rate and the wavenumber of the disturbance (the dispersion equation) is derived in a general form, although the author applied it for some particular cases. However the scope of the Tomotika equation could be extended as clearly shown in the paper of Lee and Flumerfelt (1981). In the latter an unified analysis of the Tomotika equation is proposed based on introducing different characteristic time

scales. This analysis shows that classical dispersion equations of Rayleigh and Weber mentioned above in the first group could be derived from Tomotika general equation, as well as many others, related to the second group. In the paper of Mikami and Mason (1975), the Tomotika analysis is extended on the liquid column submerged in a fluid which is contained in a tube.

It should be noted, however, that all of the abovementioned approaches remain in the scope of the linear stability theory. Furthermore it is assumed that the jet surface is disturbed by infinitely small disturbances of the form

$$\delta = \delta_0 \exp(Qt + ixz) \qquad [1]$$

where $x$ denotes the wavenumber, $Q$—growth rate, $\delta$—amplitude of the perturbation. Then the analysis of the disturbance evolution is performed by neglecting all the terms quadratic in respect to the initial amplitude $\delta_0$.

Weakly nonlinear analysis has been conducted first by Yuen (1968) for an inviscid jet of the first group. He carried out the solution up to third order in respect to $\delta_0$ and succeeded to predict the existence of satellite drops as observed by Donnelly and Glaberson (1966). Except for some one-dimensional approaches (e.g. Bogy 1979) the effect of the viscosity on nonlinear jet instability has been studied only numerically starting by the pioneering work of Shokoohi (1976) and subsequent calculations of Nichols *et al.* (1981), Fromm (1984), Bousfield *et al.* (1990), Ashgriz and Mashayek (1995). In the latter a very comprehensive review of the previous works is presented concerning liquid jets of the first group.

The papers of Hammond (1983), and Newhouse and Pozrikidis (1992) should be mentioned in the second group in which the disintegration process is studied for a configuration of a liquid column surrounded by a coaxial layer of another liquid contained in a cylindrical tube. These papers are focused mainly on the behaviour of the layer and are based on the Stokes equations of motion. In the work of Tjahjadi *et al.* (1992) the interfacial tension driven fragmentation of a very long thread filament is investigated for better understanding the role of filament instability on satellite drops size.

Our paper presents a direct simulation of the process of disintegration of a viscous liquid column in another immiscible liquid bounded by a tube. A complete numerical solution of the full Navier–Stokes equations is proposed, which gives both qualitative and quantitative results. The applicability of the numerical procedure is verified in comparison with the results of the linear stability analysis and those of Shokoohi (1976) and Shokoohi and Elrod (1987) in the case of a liquid column in an inviscid nearly-zero-density fluid. For a column in a viscous liquid phase, the verification is done on the basis of the results of Tomotika (1935) and Mikami and Mason (1975). The numerical results for the main and satellite drop sizes are compared as well to the corresponding experimental values as measured by Kitamura *et al.* (1982), when the relative velocity of both phases is maintained equal to zero.

It is shown that given disturbance of type [1] retains a cosinusoidal form at the first stages of its evolution in time. Due to the appearance of multiple harmonics the surface profile is transformed to a noncosinusoidal form, which contains a satellite drop attached to the main one. The size of the satellite is strongly connected to the wavelength. The amplification rate of the temporally growing disturbances is time dependent except for the initial time interval.

## 2. PHYSICAL MODEL AND EQUATIONS

We study the liquid column instability in respect to the so-called temporally growing disturbances. That is, the liquid column is infinite in both directions (it has neither beginning nor end). More than that, the disturbed flow is periodical along the column axis with a given wavelength $\lambda$. Both the liquid column and the surrounding fluid are supposed to be incompressible, Newtonian and immiscible. Gravity effects are neglected.

Figure 1 shows a periodic section of the axisymmetric liquid column with a single wavelength disturbance (which will be considered as fundamental or first harmonic disturbance). The continuous phase is closed at $r = R_{max}$ by a rigid cylinder. Consequently this ensures a fixed outside boundary in the computational domain. The domain is bounded elsewhere by the axis of symmetry

Oz and two cross-sections at a distance one wavelength of the prescribed disturbance. However the influence of the wall on the column instability characteristics remains to be studied.

Owing to the symmetry of the problem the hydrodynamic equations are written in a cylindrical coordinate system with $z$ and $r$ being the corresponding axial and radial coordinates. The undisturbed liquid column radius $R_N$, and the capillary time $t_0 = \sqrt{\rho_1 R_N^3/\sigma_{12}}$ are chosen as characteristic length and time respectively. Hence the pressure is scaled according to the quantity $\sigma_{12}/R_N$. Hereafter, the streamfunction-vorticity formulation of the equations will be used. The stream function $\psi$ and the vorticity $\omega$ are defined as

$$U_j = -\frac{1}{r}\frac{\partial \psi_j}{\partial r}, \quad V_j = \frac{1}{r}\frac{\partial \psi_j}{\partial z} \tag{2}$$

$$\omega_j = \frac{\partial V_j}{\partial z} - \frac{\partial U_j}{\partial r} \tag{3}$$

where $U$ and $V$ are the axial and radial components of the velocity, respectively. In [2] and [3], subscript $j = 1$ refers to the liquid column, while $j = 2$ refers to the continuous phase. Subscript $j$ will be omitted when admissible.

### 2.1. *Nondimensional governing equations*

Vorticity transport equation could be written in the following form

$$\frac{\partial \omega}{\partial t} + V\frac{\partial \omega}{\partial r} + U\frac{\partial \omega}{\partial z} - \mathrm{Oh}_1\left(\frac{\nu}{\nu_1}\right)\left[\frac{\partial^2 \omega}{\partial r^2} + \frac{1}{r}\frac{\partial \omega}{\partial r} - \frac{\omega}{r^2} + \frac{\partial^2 \omega}{\partial z^2}\right] = \frac{\omega}{r^2}\frac{\partial \psi}{\partial z} \tag{4}$$

where $\mathrm{Oh}_1$ is the liquid column Ohnesorge number ($\mathrm{Oh}_1 = \mu_1/\sqrt{\rho_1 R_N \sigma_{12}}$). Vorticity $\omega$ is connected to the stream function $\psi$ by the expression

$$\omega = \frac{1}{r}\left(\frac{\partial^2 \psi}{\partial z^2} - \frac{1}{r}\frac{\partial \psi}{\partial r} + \frac{\partial^2 \psi}{\partial r^2}\right). \tag{5}$$

The above-mentioned equations must be applied for both the liquid column and the continuous phase.

### 2.2. *Boundary conditions at the interface*

Using the kinematic requirement that the surface of the liquid column has to be constituted of the same liquid particles, one obtains the equation for the radius $R_s$ of the form

$$\frac{\partial R_s}{\partial t} + U_s\frac{\partial R_s}{\partial z} = V_s \tag{6}$$

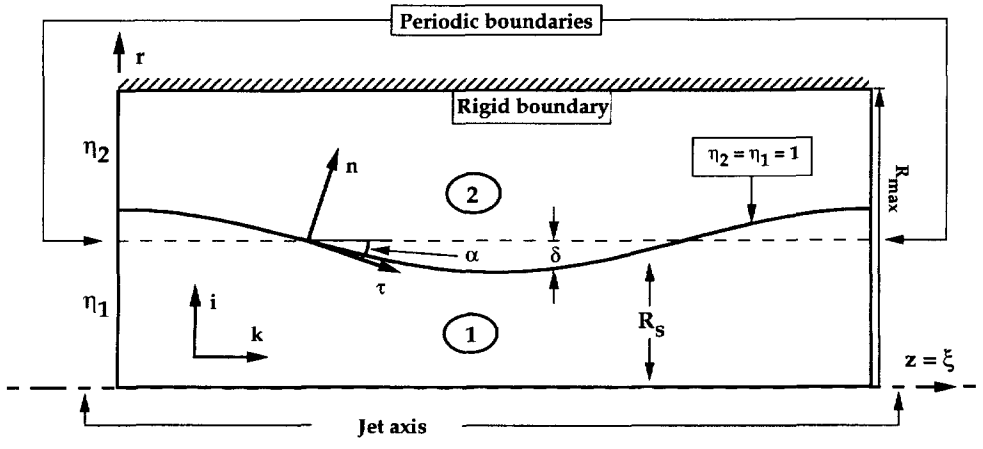


Figure 1. Geometry of the flow under consideration: a periodic section of the axisymmetric jet with a single wavelength disturbance. The continuous phase is closed at $r = R_{max}$ by a rigid cylinder.

where $R_s$ is considered as a function of the time $t$ and axial coordinate $z$. Subscript s will be used for the points at the column surface. At the latter both nonslip and zero-mass flux condition must be satisfied

$$[\![U]\!] = 0 \tag{7}$$

$$[\![V]\!] = 0 \tag{8}$$

where by definition

$$[\![G]\!] = G_{1s} - G_{2s}. \tag{9}$$

Additional conditions follow from the balance of tangential and normal stresses at the both sides of the interface, provided surface tension is taken into account. Thus for tangential stress condition we have

$$\left[\!\!\left[ \frac{\mu}{\mu_1}\left[\left(\frac{\partial V}{\partial r} - \frac{\partial U}{\partial z}\right)\sin 2\alpha + \left(\frac{\partial V}{\partial z} + \frac{\partial U}{\partial r}\right)\cos 2\alpha \right]\right]\!\!\right] = 0 \tag{10}$$

where $\alpha$ (as shown in figure 1) is the angle between the tangential unit vector $\tau$ and the axial direction. The corresponding normal stress condition is

$$\left[\!\!\left[ P - \mathrm{Oh}_1\left(\frac{\mu}{\mu_1}\right)\left[ 2\left(\frac{\partial V}{\partial r}\cos^2\alpha + \frac{\partial U}{\partial z}\sin^2\alpha\right)\right.\right.\right.$$

$$\left.\left.\left. -\left(\frac{\partial V}{\partial z} + \frac{\partial U}{\partial r}\right)\sin 2\alpha \right]\right]\!\!\right] = \left(\frac{\cos\alpha}{R_s} - \frac{\partial^2 R_s}{\partial z^2}\cos^3\alpha\right). \tag{11}$$

Because of the presence of the surface tension term in the right-hand side of [11], the pressure difference $[\![P]\!]$ could not be easily eliminated as requested by $\psi - \omega$ form of Navier–Stokes equations. To do so, [11] must be differentiated along the surface with the pressure derivatives being substituted by their expressions through Navier–Stokes equations. It should be mentioned that this transformation involves time derivatives of the velocity components in the boundary condition [11]. (For more details concerning condition [11], see appendix B.)

### 2.3. *Boundary conditions at external boundaries*

Due to the symmetry of the flow and the boundedness of the velocity, at the column axis ($r = 0$) the following conditions could be imposed

$$\omega_1 = 0 \tag{12}$$

$$\psi_1 = 0. \tag{13}$$

At the wall ($r = R_{\max}$) the zero-slip and zero-mass flux conditions must be satisfied:

$$\omega_2 = \frac{1}{r}\left(\frac{\partial^2 \psi_2}{\partial r^2}\right) \tag{14}$$

$$\psi_2 = 0. \tag{15}$$

### 2.4. *Periodicity boundary condition*

At the ends of a liquid column segment of one wavelength,

$$F(0, r, t) = F(\lambda, r, t) \tag{16}$$

is imposed, where $F$ is any flow dependent variable or its derivative.

### 2.5. *Initial condition*

The instability of the liquid column in respect to disturbances of small amplitudes could be easily obtained by analysing the linearized form of the equations and boundary conditions presented above. For the particular case of unbounded continuous phase, Tomotika (1935) derived an analytical solution of the problem as well as the corresponding dispersion relation, connecting the amplification rate $Q$ to the wavenumber $x$. When this solution is applied, the disintegrated column appears as a chain of drops of uniform size. However, the observations of the jet breakup show that the larger drops are separated by smaller ones, usually called satellites. The appearance of the latter could be attributed to the nonlinear terms in the equations of motion and in the boundary conditions at the moving interface.

On the basis of the preceding discussion we have assumed that the initial perturbation of the column appears in the form predicted by the linear instability analysis. For simplicity the initial perturbation is taken in the form of a single harmonic (see [1]), although any combination of harmonics could be involved. The dispersion equation (see [26] below) as well as the corresponding initial vorticity and stream functions are derived from linearized equations and boundary conditions.

## 3. NUMERICAL PROCEDURE

In what follows we will focus our attention on numerical solution of the governing equations as they appeared in the preceding section. This solution is based on the application of the method developed by Peaceman and Rachford (1955) known as Alternating Direction Implicit method (ADI). In particular, the ADI method has been successfully used by Shokoohi (1976) and Shokoohi and Elrod (1987) for solving the vorticity transport equation inside the jet. We have extended the method to the continuous phase vorticity equation, as well as for treating the stream function–vorticity relation in both phases. The spatial derivatives in [19] and [20] below are alternatively treated implicitly at one-half time step and explicitly at the next half-step. Using centered-difference approximations we have obtained tridiagonal systems of linear algebraic equations along each coordinate line which is solved by Thomas algorithm. A cyclic elimination method is implemented in the $\xi$-direction to exploit the periodicity of the boundary condition in this direction. In the vorticity transport equation the $\omega$ term is treated following the procedure implemented by Ryskin and Leal (1984). Although at the end of this section the sequence of the steps of the numerical algorithm is listed, some details still remain to be discussed.

As a first step toward the numerical procedure we replace the radial coordinate $r$ by the new independent variables

$$\eta_j = \frac{(j-1)R_{\max} - r}{(j-1)R_{\max} - R_s} \qquad [17]$$

where $0 \leqslant \eta_1 \leqslant 1$ and $1 \geqslant \eta_2 \geqslant 0$, and simply introduce new symbols for the time and axial coordinate

$$\tau = t, \quad \xi = z. \qquad [18]$$

The transformation [17] enables us to avoid the use of deformable mesh, keeping one of the mesh lines fixed along the interface. Using the new coordinate system one obtains:

Vorticity transport equation in the form

$$\frac{\partial \omega}{\partial \tau} = a_1 \frac{\partial^2 \omega}{\partial \eta^2} + a_2 \frac{\partial \omega}{\partial \eta} + a_3 \frac{\partial^2 \omega}{\partial \eta\, \partial \xi} + a_4 \frac{\partial \omega}{\partial \xi} + a_5 \frac{\partial^2 \omega}{\partial \xi^2} + a_6 \omega, \qquad [19]$$

$\psi$–$\omega$ relation

$$b_1 \frac{\partial^2 \psi}{\partial \eta^2} + b_2 \frac{\partial \psi}{\partial \eta} + b_3 \frac{\partial^2 \psi}{\partial \eta\, \partial \xi} + \frac{\partial^2 \psi}{\partial \xi^2} = r\omega \qquad [20]$$

Velocity components

$$V = g_1 \frac{\partial \psi}{\partial \xi} + g_2 \frac{\partial \psi}{\partial \eta}, \quad U = g_3 \frac{\partial \psi}{\partial \eta}. \tag{21}$$

The above written equations stand for both the dispersed and the continuous phases. The coefficients $a_1$, $b_1$ and $g_1$ as well as the transformation matrix of the derivative operators are given in appendix C and appendix A, respectively. It is worth noting that mixed derivatives have appeared in [19] and [20], being a result of the nonorthogonality of the new coordinate system. In our method, these derivatives are treated explicitly.

The corresponding conditions at the interface are written in respect to the same independent variables:

Tangential stress condition

$$\left[\!\left[ c_1 \frac{\partial^2 \psi}{\partial \eta^2} + c_2 \frac{\partial \psi}{\partial \eta} + c_3 \frac{\partial^2 \psi}{\partial \eta \, \partial \xi} + c_4 \frac{\partial \psi}{\partial \xi} + c_5 \frac{\partial^2 \psi}{\partial \xi^2} \right]\!\right] = 0, \tag{22}$$

Modified normal stress condition

$$\left[\!\left[ \sum_{k=1}^{k=9} d_k D_k^{\eta,\xi} \psi \right]\!\right] = s. \tag{23}$$

The kinematic condition [6] is now transformed to

$$\frac{\partial R_s^2}{\partial \tau} = 2 \left. \frac{\partial \psi}{\partial \xi} \right|_{\eta = 1} \tag{24}$$

as well as the boundary condition [14]

$$\omega_2 = b_W \frac{\partial^2 \psi_2}{\partial \eta_2^2}. \tag{25}$$

The remaining conditions [12], [13], [15] and [16] are of the same form but they must be applied for the corresponding value of $\eta$.

For the equations and boundary conditions, we use a uniform finite-difference grid of step sizes $\Delta\eta$ and $\Delta\xi$ in corresponding directions. The scheme is centered in space and forward in time. The method is necessarily iterative due to the dependence of the coefficients $a_1$, $b_1$, $c_1$, $d_1$ and $g_1$ on the unknown column radius [24] and its derivatives up to the third order. As mentioned above the initial approximation of the column radius is of the form [1]. Then the numerical solution follows time evolution of the initial disturbance which remains periodical in axial direction. At any time step the updated radius is differentiated numerically by using cubic splines.

Here follows the (iterative) numerical procedure:

Step 1: increase the time.

Step 2: compute a new surface profile $R_s$ using the kinematic condition [24].

Step 3: differentiate $R_s$.

Step 4: solve the vorticity transport equation [19, $j = 1$] for the column (the vorticity values of the preceding iteration are used at the interface).

Step 5: solve the vorticity transport equation [19, $j = 2$] for the continuous phase.

Step 6: approximate the vorticity on the rigid wall using the nonslip condition [25].

Step 7: solve the $\psi$–$\omega$ relation [20, $j = 1$] for the stream function in the column (a pseudo-transient approach is used by adding a fictitious time derivative of $\psi$ in $\psi$–$\omega$ relation. This enables us to transform the latter to a form convenient for using ADI method).

Step 8: solve the $\psi$–$\omega$ relation [20, $j = 2$] for the stream function in the continuous phase.

Step 9: determine the column vorticity at the interface using tangential stress equation [22].

Step 10: determine the continuous phase vorticity at the interface by approximating the corresponding $\psi$–$\omega$ relation [20, $j = 2$] on the interface.

Step 11: compute the velocity component values [21] everywhere.

Step 12: determine the stream function value at the interface using the modified normal stress condition [23].

Step 13: go to step 2 if the convergence criterion is not satisfied (if necessary reduce the time step and correct the total time); go to step 1 if the time step is not less than a given value.

Stop.

## 4. RESULTS

### 4.1. Numerical strategy

Since the column radius $R_s$ depends on the values of $\psi$ at the column surface, the iterations in $\psi$ and $\omega$ are coupled to the iterations in the interface position. Similar coupling has been successfully implemented by Asaithambi (1993). For the current time step the calculation is terminated whenever $\varphi \leqslant \epsilon$ with $\varphi = \max_F(\varphi_F)$, where $\varphi_F = \max_{i,k}(|F^s_{i,k} - F^{s-1}_{i,k}|)$ is the maximum error in the 'field' of $F$ related to two consecutive iterations. Here $F$ denotes any of the unknowns of the problem while $F^s_{i,k}$ is the corresponding grid function related to the $s$th iteration. In some cases, to preserve the solution from very abrupt variations it is necessary to reduce the time increment mainly near the column breakup time. Then the time step is divided by two whenever a given number of iterations is attained before the above accuracy criterion is satisfied. The calculation ends off for a given case when the time step becomes too small ($\Delta\tau \approx 10^{-5}$). At this stage in general, the nondimensional radius of the column at the minimal cross-section is less than 0.05 (in some cases, the minimal radius is of about 0.005): the corresponding section and total time are considered as breakup point and time, respectively. For all computations performed with the chosen $\Delta\eta$, $\Delta\xi$, and $\Delta\tau$, no indication of numerical instability has been noticed. Tests for accuracy have been performed according to Shokoohi (1976): a twofold variation in $\Delta\xi$ and a fivefold variation in $\Delta\tau$ make no significant difference. Typically we use $\epsilon = 10^{-6}$ and initial time step $\Delta\tau = 0.05$. Concerning the space steps, for all the cases presented here we have $\Delta\eta_1 = 0.1$, $\Delta\eta_2 = 0.025$; $\Delta\xi = 0.5$ for $x < 0.7$ and $\Delta\xi = \lambda/20$ for $x \geqslant 0.7$.

Further on we present the results obtained for two liquid–fluid systems. The first system concerns a water column in a low density nonviscous gas referred below as water–gas system. The latter is used to test our results to some available experimental and numerical results of other authors.

In the second system the column of water is submerged in another immiscible liquid; in particular dodecan. Some selected examples of the behaviour of the unstable column are discussed. Present numerical results are compared with the experimental results of Mikami and Mason (1975) and Kitamura *et al.* (1982).

### 4.2. Liquid–gas system

The characteristic parameters of the system are given in appendix D. The value of the column radius is $R_N = 0.00175$ cm and the initial amplitude in [1] is $\delta_0 = 0.02$. The initial stream and vorticity functions are evaluated using Weber (1931) solution.

Figure 2 compares two column profiles for the wavenumber ($x \approx 0.7$) related to the maximal growth rate in linear theory approximation. One (solid line) is obtained by Shokoohi (1976), the other (dash line)—by our approach. The comparison shows close agreement between the shapes of the interfaces. The error in the final (or breakup) times is less than 2%.

One of the basic characteristics of the column instability is the time interval in which the column remains unbroken, known as breakup time. (The latter could be easily related to the unbroken jet length, a parameter widely used in many applications.) Several curves 'wavenumber–breakup time' are plotted in figure 3 in order to compare our and Shokoohi (1976) numerical results. The breakup times show a close agreement. In the same figure we display the breakup times given by the linear stability analysis (here particularly—by the Weber 1931 solution), as well as the corresponding dispersion $x$–$Q$ curve. The shortest breakup time is found approximately at $x = 0.7$, which is in accordance to the classical Rayleigh result (note that the water viscosity is relatively small).

The growth rate curve has a maximum at $x \approx 0.7$. According to the linear theory analysis there is no amplification of the perturbation for $x = 0$ (wavenumber of the infinite wavelength) and $x = 1$ (the cut-off wavenumber). However in the nonlinear simulation, we observed some growing of the

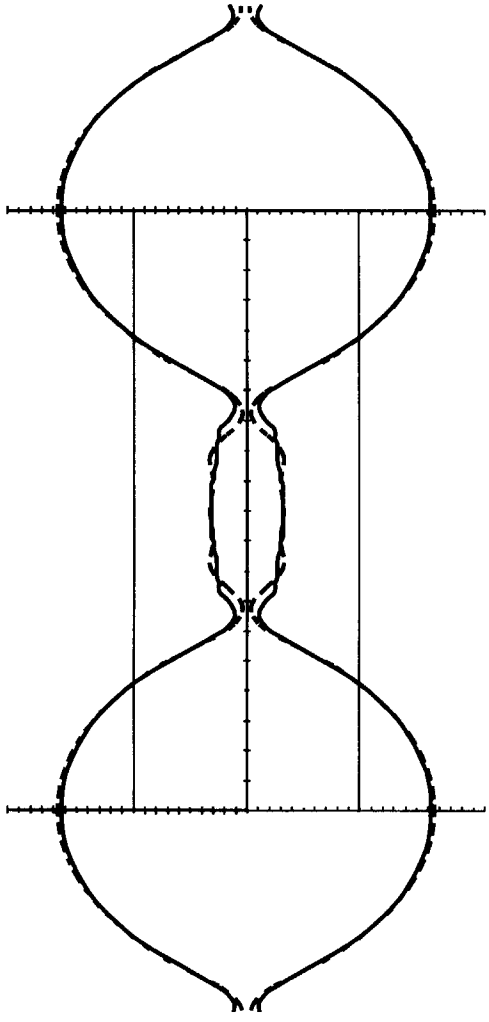

Figure 2. Instantaneous interface profile proceding column breakup. (Water–gas system: $\delta_0 = 0.02$, $R_N = 0.00175$ cm; $Oh_l = 0.028$.) – – – $x = 0.70$, $T = 10.75$: present result. —— $x = 0.70$, $T = 10.96$: Shokoohi (1976, 1987).

perturbation at the cut-off wavelength with an 'infinitely small amplification rate' (not shown). Similar effect was observed by Shokoohi (1976).

An additional comparison between the present and the numerical solution of Shokoohi (1976) will be shown below (see figure 10) for the sizes of the generated drops.

### 4.3. *Liquid–liquid system*

The basic system we use in the calculations is water–dodecan, whose characteristic parameters are shown in appendix D.

The values of $R_N$ and $\delta_0$ are the same as in the preceding section. The initial stream and vorticity functions are based on modified Tomotika (1935) solution. The modification is necessary for incorporating into the solution the radius $R_{max}$ of the rigid tube confining the continuous phase. The modified dispersion equation could be written in the form

$$\begin{vmatrix} I_1(x) & I_1(x_1) & K_1(x) & K_1(x_2) & I_1(x) & I_1(x_2) \\ xI_0(x) & x_1I_0(x_1) & -xK_0(x) & -x_2K_0(x_2) & xI_0(x) & x_2I_0(x_2) \\ 2x^2I_1(x) & (x^2+x_1^2)I_1(x_1) & 2\mu^*x^2K_1(x) & \mu^*(x^2+x_2^2)K_1(x_2) & 2\mu^*x^2I_1(x) & \mu^*(x^2+x_2^2)I_1(x_2) \\ F_1 & F_2 & F_3 & F_4 & F_5 & F_6 \\ 0 & 0 & K_1(y) & K_1(y_2) & I_1(y) & I_1(y_2) \\ 0 & 0 & -yK_0(y) & -y_2K_0(y_2) & yI_0(y) & y_2I_0(y_2) \end{vmatrix} = 0 \quad [26]$$

where

$$\mu^* = \frac{\mu_2}{\mu_1}, \quad \rho^* = \frac{\rho_2}{\rho_1}$$

$$x_1 = \sqrt{x^2 + \frac{Q}{\mathrm{Oh}_1}} \quad x_2 = \sqrt{x^2 + \frac{Q}{\mathrm{Oh}_1}\frac{\nu_1}{\nu_2}} \quad y = xR_{\max} \quad y_2 = x_2 R_{\max}$$

$$F_1 = Q^2 I_0(x) + 2x^2 \mathrm{Oh}_1 Q I_1'(x) + x(x^2 - 1) I_1(x) \quad F_2 = 2xx_1 \mathrm{Oh}_1 Q I_1'(x_1) + x(x^2 - 1) I_1(x_1)$$

$$F_3 = 2x^2 \mu^* \mathrm{Oh}_1 Q K_1'(x) - \rho^* Q^2 K_0(x) \quad F_4 = 2xx_2 \mu^* \mathrm{Oh}_1 Q K_1'(x_2)$$

$$F_5 = 2x^2 \mu^* \mathrm{Oh}_1 Q I_1'(x) + \rho^* Q^2 I_0(x) \quad F_6 = 2xx_2 \mu^* \mathrm{Oh}_1 Q I_1'(x_2).$$

In [26], $I_n(\zeta)$ and $K_n(\zeta)$ are the modified Bessel functions of $n$th order, while $I_n'(\zeta)$ and $K_n'(\zeta)$ denote their first derivatives in respect to $\zeta$. This dispersion equation is equivalent to the dispersion equation obtained by Mikami and Mason (1975). When $R_{\max} \to \infty$, [26] is reduced to the general Tomotika (1935) dispersion relation (for more details, see also Lee and Flumerfelt 1981).

When [26] is solved the growth rate $Q$ could be expressed as a function of the wavenumber or any other of the nondimensional parameters. In figure 4 the variation of $Q$ with $R_{\max}$ is plotted for selected values of the wavenumber. The effect of the wall on the numerical solution is illustrated in figure 5.

These figures show that the wall plays no role in the column instability when $R_{\max} \geqslant 5$. Further on, the value of $R_{\max}$ is set equal to 5 along all the computations.

An example of the evolution of the interface profile in time is shown in figure 6 for $t = 0$–12.51. The wavelength corresponds to that of the fastest growing disturbance. In the early stages, the surface contour has only one minimum at exactly $\lambda/2$. As the time increases, nonlinearities become important and the initially cosinusoidal shape of the interface changes to a more complex form. The zone of the minimum passes progressively through a 'plateau', then two equal minima develop on both sides of $\lambda/2$ and move symmetrically toward the wavelength ends, giving rise to a satellite drop.

From the experiments of Mikami and Mason (1975) it could be expected that the amplitude of

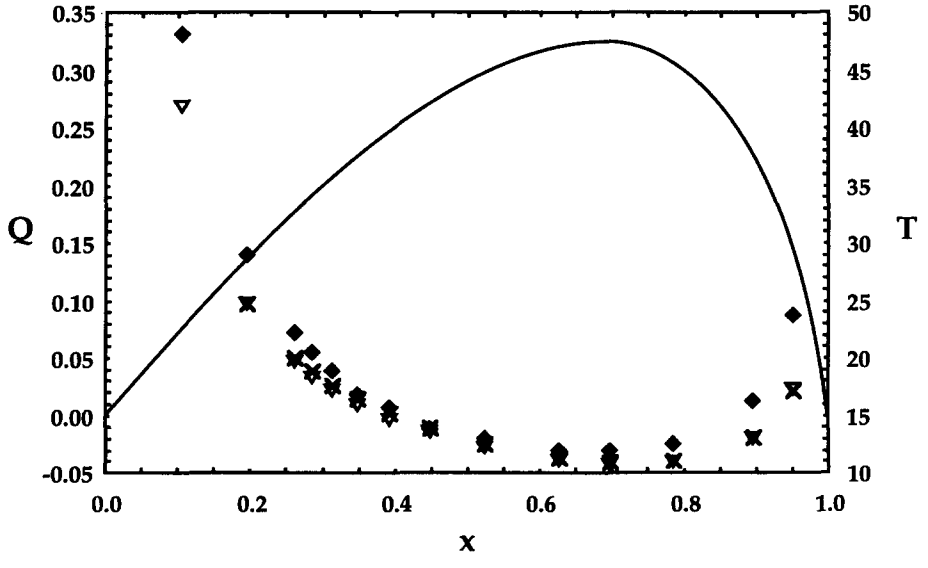


Figure 3. Nondimensional growth rate $Q$ and breakup time $T$ vs nondimensional wavenumber $x$. (Water–gas system: $\delta_0 = 0.02$, $R_N = 0.00175$ cm; $\mathrm{Oh}_1 = 0.028$.) $Q$: —— Linear theory (Weber 1931). $T$: ▽ Present results; ◆ Weber's results; × Shokoohi's results.

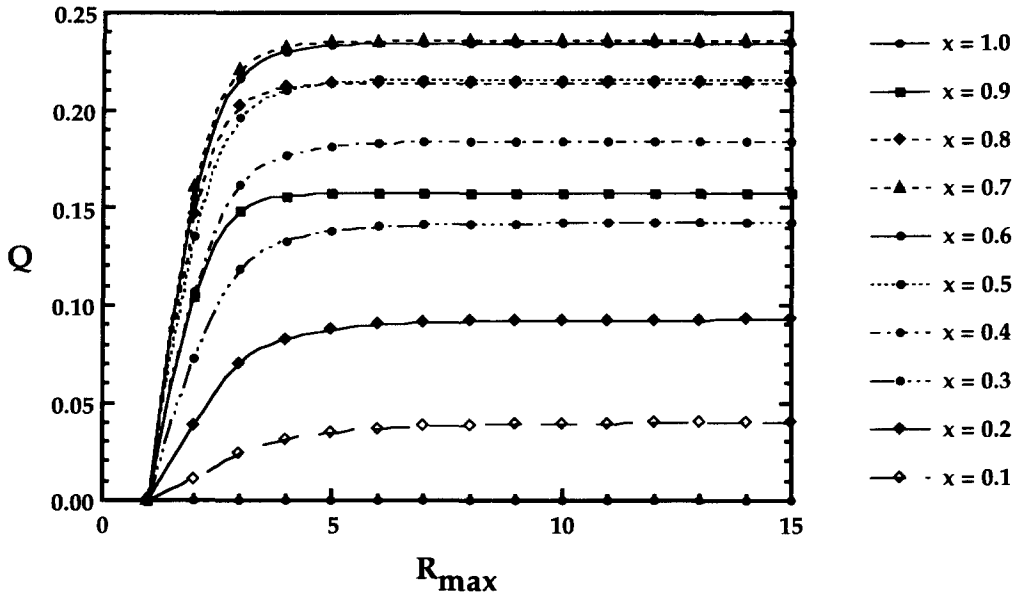


Figure 4. Variation of the nondimensional growth rate $Q$ in linear theory approximation with the nondimensional radius of the rigid cylinder $R_{max}$ bounding the continuous phase at different nondimensional wavenumbers $x$ (water–dodecan system: $Oh_1 = 0.031$).

the initial being as well as a cosinusoidal disturbance will grow (at least at the beginning) with the growth rate predicted by the linear theory for the same wavenumber. To test this in figure 7 the calculated amplitudes of the neck and the swell of the disturbance are shown as functions of time at two different wavenumbers of the range of short wavelengths. Continuous (straight) lines represent the corresponding amplitudes predicted by the linear theory solution [1]. Combining the observations of figures 6 and 7 it could be concluded that the evolution of the disturbances along the initial time interval ($t \leqslant 5$ in figure 7) is well predicted by the linear instability analysis.

The curves $t$–$\delta$ (for a given cross-section) based on the present numerical solution could be used

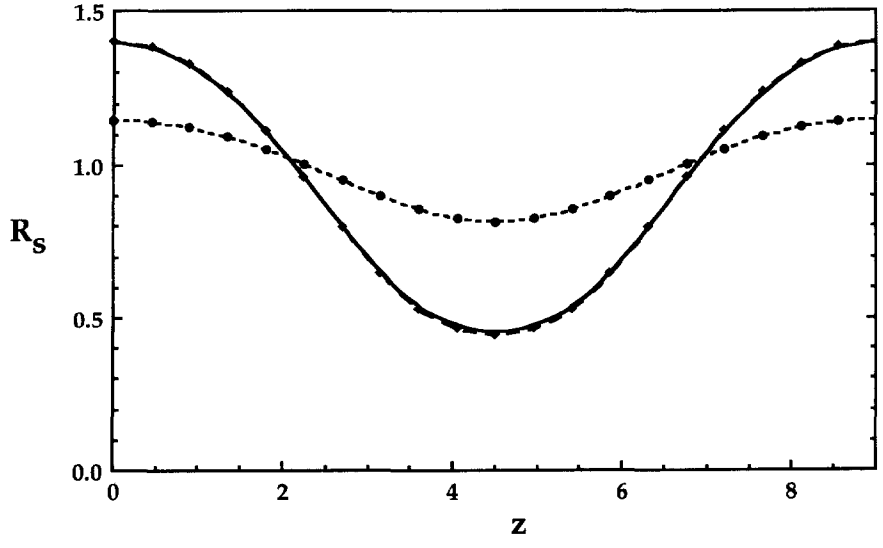


Figure 5. Effect of the position of the rigid wall on the jet instability: interface profiles for different values of $R_{max}$ at $t = 11.25$. ('Water–dodecan': $\delta_0 = 0.02$, $x = 0.70$, $R_N = 0.00175$ cm; $Oh_1 = 0.031$) —●— $R_{max} = 2$; —— $R_{max} = 5$; —◆— $R_{max} = 9$.

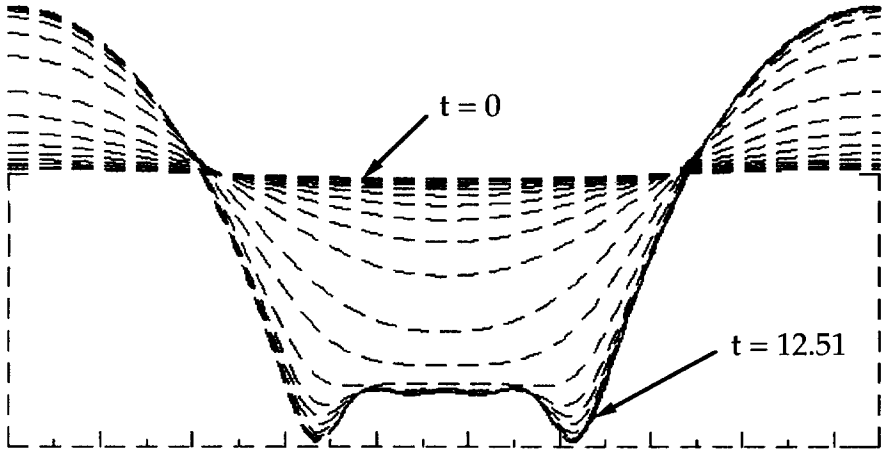


Figure 6. Evolution of the interface in time. ('Water–dodecan': $\delta_0 = 0.02$; $x = 0.66$; $R_N = 0.00175$ cm; $Oh_1 = 0.031$.) Three stages are observed: cosinusoidal evolution, appearance of a 'plateau', formation of a satellite and breakup.

for determining the 'instantaneous' growth rate

$$Q = \frac{\partial}{\partial t}(\ln \delta) \qquad [27]$$

at a given time $t$ for a given wavenumber $x$.

This equation allows us to test whether our numerical solution reproduces the growth rates derived in the experiments of Mikami and Mason (1975). In figure 8 the experimental points correspond to two different liquid–liquid systems A and B whose characteristic parameters are shown in appendix D. (Note that in these experiments the jet radius is variable, while the tube (rigid cylinder) radius remains fixed.) The growth rates based on the numerical solution are in a close agreement to those related to the experiments.

The above conclusion equally concerns the ratio $1/R_{max} = 0.2$ we are interested in as well as the other values of this parameter involved in the discussed experiments.

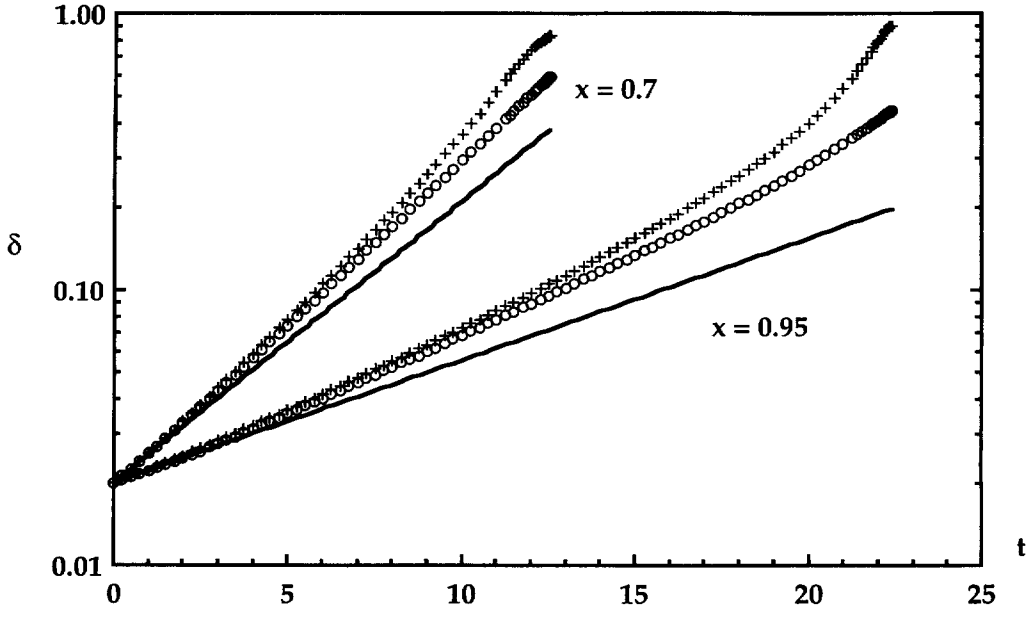


Figure 7. Growth of the disturbance amplitude in time for a water–dodecan system. ($\delta_0 = 0.02$, $R_N = 0.00175$ cm; $Oh_1 = 0.031$.) Linear solution: —— Numerical solution: + neck; ○ swell.

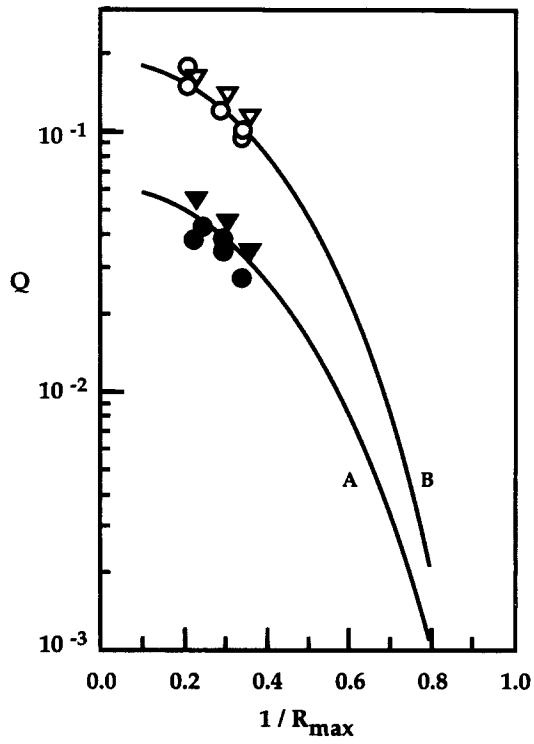


Figure 8. Nondimensional growth rate $Q$ as a function of the nondimensional radius of the tube $R_{max}$. ($R_N R_{max} = 0.05$ cm; (A): $\mu_2/\mu_1 = 0.68$; (B): $\mu_2/\mu_1 = 6.74$.) ○, ●: experimental points (Mikami and Mason 1975). ▽, ▼: numerical points (present work). The lines drawn are obtained from the linear theory [26].

Figure 9 is similar in figure 3, however concerns a liquid–liquid system and in a sense supplements figure 7. The latter indicates that, in general, the nonlinear effects accelerate the breaking of the column (i.e. reduce the break-up time in respect to its linear theory value), a tendency, which in figure 9 is demonstrated for all unstable wavenumbers. This tendency is more pronounced for the liquid–liquid system, than for, the liquid–gas system (see figure 3), owing to the fact that the

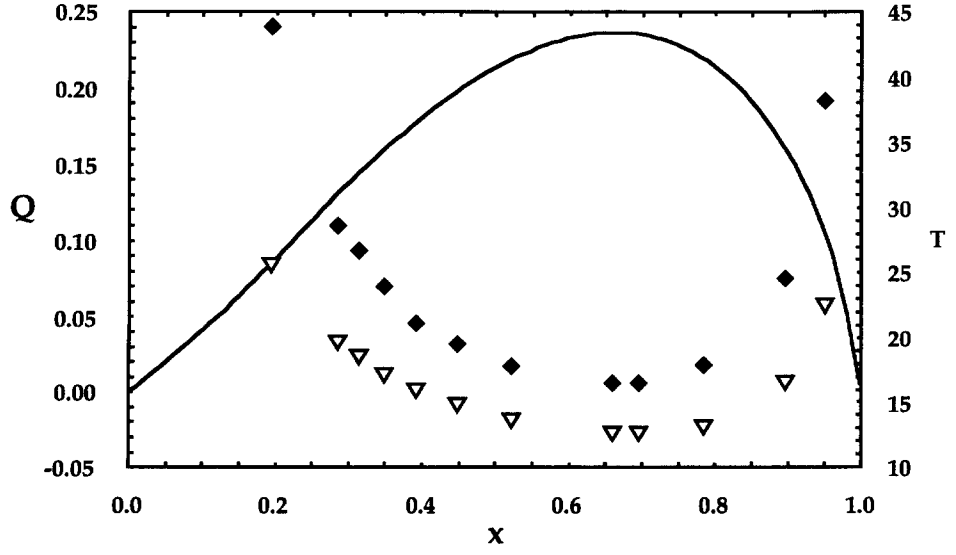


Figure 9. Nondimensional growth rate $Q$ and nondimensional breakup time $T$ vs nondimensional wavenumber $x$. (Water–dodecan system: $\delta_0 = 0.02$, $R_N = 0.00175$ cm; $Oh_1 = 0.031$.) $Q$: —— Linear theory. $T$: ▽ Direct simulation; ◆ Linear theory.

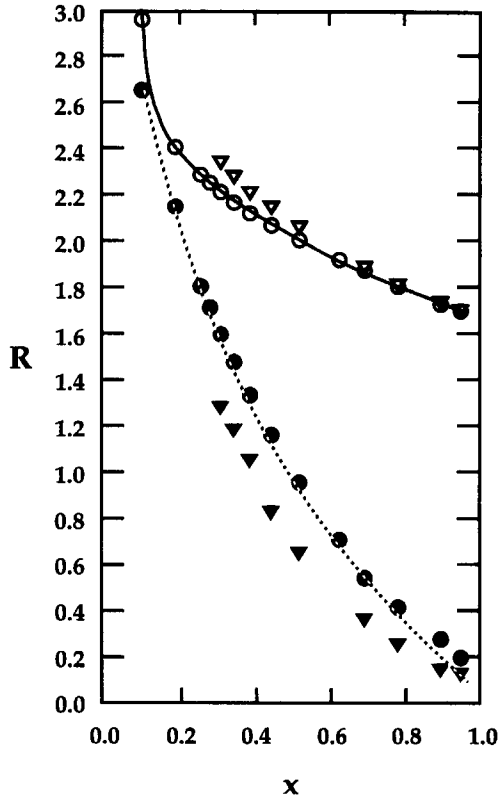


Figure 10. Nondimensional drops radii $R$ vs nondimensional wavenumber $x$: water–dodecan system (present): ▽ main drop, ▼ satellite drop. Water–gas system: ○ main drop, ● satellite drop (present work), —— main drop, – – – satellite drop (Shokoohi).

breakup times for the latter are shorter. However the wavenumber related to the minimal growth rate is one and the same both in linear and nonlinear approximation.

One of the most interesting for the applications of the liquid jets is the size distribution of the drops resulting in the breakup versus the wavenumber. After determining the positions of the two breakup points along the wavelength, the volumes of the liquid contained in the main and satellite drops are calculated. The drops volumes are converted into the drops radii, assuming that the resulting drops will be spherical. Predicted distributions of the drops are shown in figure 10 for both systems: water–gas and water–dodecan. Our results for the water–gas system are compared (see continuous and dash lines) to those of Shokoohi (1976) and show close agreement. Another comparison is presented in table 1, in which the main drops radii related to the present numerical method are compared to the experimental radii measured by Kitamura *et al.* (1982) for selected liquid–liquid systems. It should be mentioned that in these experiments the relative velocity between the phases has been maintained at different values: the present direct simulations correspond to the case of zero relative velocity.

Table 1. Main drops diameter Ø: comparison between the experimental (Kitamura *et al.* 1982) and numerical (present) results. $R_N = 0.043$ cm for system 4–1 ($Oh_l = 0.003$) and $R_N = 0.061$ cm for the systems 1–1 ($Oh_l = 0.003$), 3–2 ($Oh_l = 0.130$), 6–1 ($Oh_l = 0.054$). The deviation between numerical and experimental results is less than 10%. The volume of the satellite drop $v_{sat}$ is negligible in comparison to that of the column $v_{tot}$. (For the characteristic parameters of the systems, see appendix D.)

| System no. | $\lambda$ (—) | $v_{sat}/v_{tot}$ (%) | $\phi$ experimental (cm) | $\phi$ numerical (main drop) (cm) | Error ($\phi$) (%) |
|---|---|---|---|---|---|
| 1–1 | 9.41 | 0.53 | 0.237 | 0.234 | 1.27 |
| 3–2 | 10.28 | 1.83 | 0.250 | 0.240 | 4.0 |
| 4–1 | 9.61 | 0.32 | 0.183 | 0.168 | 8.2 |
| 6–1 | 9.9 | 1.06 | 0.255 | 0.236 | 7.45 |

Table 2. Effect of the initial amplitude on drops sizes ($R_N = 0.00175$ cm, $x = 0.5$). Liquid 1–Liquid 1: $Oh_l = 0.031$; Liquid 3–Liquid 1: $Oh_l = 0.001$

| System | $\delta_0$ (—) | Satellite drop radius (—) | Main drop radius (—) | $v_{sat}/v_{tot.}$ (%) |
|---|---|---|---|---|
| 'Liquid 3–Liquid 1' | 0.2 | 0.783 | 2.078 | 5.07 |
| | 0.1 | 0.854 | 2.067 | 6.58 |
| | 0.02 | 0.930 | 2.052 | 8.52 |
| | 0.001 | 0.937 | 2.051 | 8.69 |
| | 0.0001 | 0.937 | 2.051 | 8.69 |
| 'Liquid 1–Liquid 1' | — | — | — | — |
| | 0.1 | 0.659 | 2.093 | 3.03 |
| | 0.02 | 0.696 | 2.089 | 3.57 |
| | 0.001 | 0.697 | 2.089 | 3.59 |
| | 0.0001 | 0.697 | 2.089 | 3.59 |

In figure 10 it could be observed, that the drops size is mainly related to the wavenumber, when all other nondimensional parameters remain fixed. In the neighbourhood of the wavenumber related to the maximal growth rate (see figure 9) the satellite radius is comparatively small and the volumes of the liquid column and main drops differ slightly. An idea about this difference could be drawn from the third column of the table 1, where the volume of the satellites (not reported in Kitamura *et al.* 1982) is related to the total volume of the column (the latter could be easily determined in $cm^3$ by adding together the corresponding volumes of the third and fifth columns of table 1). In a connection to the table 1 the effect of the initial amplitude on the drop sizes remains to be studied. In table 2 this effect is shown for two liquid–liquid systems which differ from each other by the density of the column: the density of Liquid 3 is 10 times higher than that of Liquid 1. Sufficiently small amplitudes do not change significantly the satellite drop size. However after some critical value of the initial amplitude (in our simulations $\delta_0 = 0.2$) the size of the satellite is reduced more appreciably. Similar observations have been reported in the paper of Ashgriz and Mashayek (1995). In table 2 this effect is more pronounced for the system Liquid 3–Liquid 1, whose breakup times are higher.

The introduction of the effects of the continuous phase increases the number of the nondimensional parameters of the problem; from three for liquid–gas systems to six for liquid–liquid systems. The first three parameters (Ohnesorge number, wavenumber and initial amplitude) could be varied independently of the properties of the continuous phase. The next three parameters (densities, viscosities and cylinder-to-column radii ratios) stand for the continuous phase effects. In the present paper we do not intend to display all the results, obtained by a systematical variation of the parameters. An idea about the influence of the continuous phase density on the column instability could be derived from figure 11. Here the interface profiles before breaking are drawn for three different values of the densities ratio. In general, with the decreasing of the continuous phase density (at fixed other parameters) the satellite volume (as well as the radius) increases while for the breakup time, the opposite tendency is observed. It should be mentioned that in our computations the range of the Ohnesorge number remains rather limited, due to the fact that the viscosity of the column is of the order of the water viscosity. With the increasing of the column viscosity, the convergence of our numerical method becomes slower, the corresponding time step decreases below $10^{-5}$. For $Oh_l > 3$ the evolution of the disturbance remains within the initial cosinusoidal stage. This behaviour of the solution was observed when we attempted to determine the radii of the resulting drops for comparing them to those measured by Mikami and Mason (1975). The problem of the convergence of the present method for high viscous columns remains open.

## 5. CONCLUSION

A finite difference iterative method is developed for solving the equations of motion and boundary conditions that govern the instability and breakup of a liquid column surrounded by another immiscible fluid.

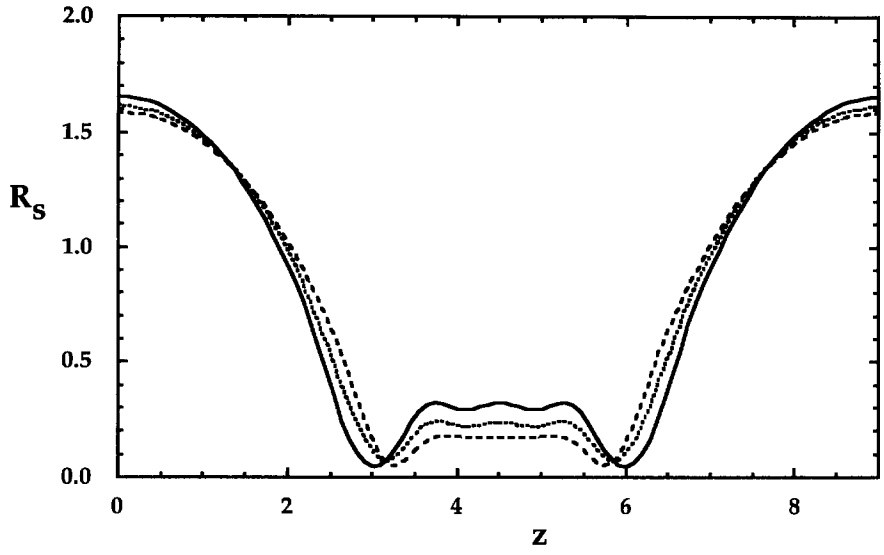


Figure 11. Effect of the continuous phase density on the column breakup. ($x = 0.70$, $\delta_0 = 0.02$, $R_N = 0.00175$ cm; $Oh_1 = 0.031$.) —— Water–dodecan, $T = 12.52$; - - - Liquid 1–Liquid 2, $T = 11.82$; — — — Liquid 1–gas, $T = 10.91$.

The numerical solution involves six nondimensional parameters: wavenumber, Ohnesorge number, initial amplitude, as well as densities, viscosities and cylinder-to-column radius ratios. The method has been applied to two selected systems: water–gas and water–dodecan for particular values of the nondimensional parameters. The full range of the parameters variation remains to be studied separately.

The water–gas system has been used as a 'test system' for the present direct simulations. The comparison shows close agreement to the numerical results of Shokoohi (1976) concerning the instantaneous interface profile, as well as the resulting main and satellite drops sizes.

Our numerical method has been tested as well to the experimental results of Kitamura *et al.* (1982), being obtained for liquid–liquid systems of zero relative velocity between the inner and the outer phases.

In general the presence of the continuous phase accelerates the appearance of the nonlinear evolution of the disturbance. However the common tendency manifested within the linear theory approximation remains unchanged: the breakup time increases when the density (respectively, viscosity) of the continuous phase increases.

## REFERENCES

Asaithambi, N. S. (1993) Numerical modeling of unsteady fluid interface. *Math. Modelling and Sci. Computing* **2,** 1177–1182.

Ashgriz, N. and Mashayek, F. (1995) Temporal analysis of capillary jet breakup. *J. Fluid Mech.* **291,** 163–190.

Bogy, D. B. (1979) Break-up of a liquid jet: second perturbation solution for one-dimensional Cosserat theory. *IBM J. Res Dev.* **23,** 87–92.

Bousfield, D., Stockel, I. H. and Nanivadekar, C. K. (1990) The breakup of viscous jets with large velocity modulations. *J. Fluid Mech.* **218,** 601–617.

Donnelly, R. J. and Glaberson, W. (1966) Experiments on the capillary instability of a liquid jet. *Proc. Roy. Soc. London* **A290,** 547–556.

Fromm, J. (1981) Finite difference computation of the capillary jet, free surface problem. *Lect. Notes Phys.* **141,** 188–193.

Hammond, P. S. (1983) Nonlinear adjustment of a thin annular film of viscous fluid surrounding a thread of another within a circular cylindrical pipe. *J. Fluid Mech.* **137,** 363–384.

Kitamura, Y., Michima, H. and Takahashi, T. (1982) Stability of jets in liquid–liquid systems. *Can. J. Chem. Eng.*, **60,** 723–731.
Lee, W.-K. and Flumerfelt, R. W. (1981) Instability of stationary and uniformly moving cylindrical fluid bodies—I. Newtonian systems. *Int. J. Multiphase Flow*, **7,** 363–383.
McCarthy, M. J. and Molloy, N. A. (1974) Review of stability of liquid jets and the influence of nozzle design. *The Chemical Engineering Journal* **7,** 1–20.
Mikami, T. and Mason, S. G. (1975) Capillary breakup of a binary liquid inside a tube. *Can. J. Chem. Eng.*, **53,** 372–377.
Newhouse, L. A. and Pozrikidis, C. (1992) The capillary instability of annular layers and liquid threads. *J. Fluid Mech.* **242,** 193–209.
Nichols, B. D., Hirt, C. W. and Hotchkiss, R. S. (1981) A fractional volume of fluid method for free boundary dynamics. *Proceedings of the Seventh International Conference on Numerical Methods in Fluid Dynamics*, pp. 98–105. Springer, Berlin.
Peaceman, D. W. and Rachford, H. H. Jr. (1955) The numerical solution of parabolic and elliptic differential equations. *J. of Society of Industrial Applied Math.* **23,** 28–41.
Rayleigh, L. (1878) On the instability of jet. *Proc. Lond. Math. Soc.* **10,** 4–13.
Ryskin, L. and Leal, L. G. (1984) Numerical solution of free boundary problems in fluid mechanics, Part 1. *J. Fluid Mech.* **148,** 1–17.
Shokoohi, F. (1976) Numerical investigation of the disintegration of liquid jets. Ph.D. thesis, Colombia University, New York.
Shokoohi, F. and Elrod, H. G. (1987) Numerical investigation of the disintegration of liquid jets. *J. Comp. Phys.* **71,** 324–342.
Tjahjadi, M., Stone, H. A. and Ottino, J. M. (1992) Satellite and subsatellite formation in capillary breakup. *J. Fluid Mech.* **243,** 297–317.
Tomotika, S. (1935) On the instability of a cylindrical thread of a viscous liquid surrounded by another viscous fluid. *Proc. R. Soc. Lond.* **A,** 322–337.
Weber, C. (1931) Zum zerfall eines flüssigkeitsstrahles. *Z. Angew, Math. Meh.* **11,** 136–154.
Yuen, M. C. (1968) Nonlinear capillary instability of a liquid jet. *J. Fluid Mech.* **33,** 151–163.

## APPENDIX A

### *Transformation Matrix*

According to the coordinate transformation $\eta_j = (R_j - r)/(R_j - R_s)$ and $\xi = z$, the derivative operators in respect to the cylindrical coordinates $(r, z)$ are expressed in respect to the new variables $(\eta_j, \xi)$ by the following matrix relation

$$\{D^{r,z}\} = [T_j]\{D^{\eta_j,\xi}\} \tag{A1}$$

where $\{D^{r,z}\}$ and $\{D^{\eta_j,\xi}\}$ are $9 * 1$ column matrices

$$\{D^{r,z}\} = \left\{\frac{\partial^3}{\partial r^3}, \frac{\partial^2}{\partial r^2}, \frac{\partial}{\partial r}, \frac{\partial^3}{\partial r^2\,\partial z}, \frac{\partial^2}{\partial r\,\partial z}, \frac{\partial^3}{\partial r\,\partial z^2}, \frac{\partial}{\partial z}, \frac{\partial^2}{\partial z^2}, \frac{\partial^3}{\partial z^3}\right\}^T \tag{A2}$$

$$\{D^{\eta_j,\xi}\} = \left\{\frac{\partial^3}{\partial \eta_j^3}, \frac{\partial^2}{\partial \eta_j^2}, \frac{\partial}{\partial \eta_j}, \frac{\partial^3}{\partial \eta_j^2\,\partial \xi}, \frac{\partial^2}{\partial \eta_j\,\partial \xi}, \frac{\partial^3}{\partial \eta_j\,\partial \xi^2}, \frac{\partial}{\partial \xi}, \frac{\partial^2}{\partial \xi^2}, \frac{\partial^3}{\partial \xi^3}\right\}^T. \tag{A3}$$

The elements of the transformation matrix $[T_j]$ are as follows

$$T_j(1, 1) = -\epsilon_j^3$$

$$T_j(2, 2) = \epsilon_j^2$$

$$T_j(3, 3) = -\epsilon_j$$

$$T_j(4, 1) = \eta_j\epsilon_j^2\gamma_j; \quad T_j(4, 2) = 2\epsilon_j^2\gamma_j; \quad T_j(4, 4) = \epsilon_j^2$$

$$T_j(5, 2) = -\eta_j\epsilon_j\gamma_j; \quad T_j(5, 3) = -\epsilon_j\gamma_j; \quad T_j(5, 5) = -\epsilon_j$$

$$T_j(6,1) = -\eta_j^2\epsilon_j\gamma_j^2; \quad T_j(6,2) = -\eta_j\epsilon_j(4\gamma_j^2 + \epsilon_j R_s''); \quad T_j(6,3) = -\epsilon_j(2\gamma_j^2 + \epsilon_j R_s'')$$

$$T_j(6,4) = -2\eta_j\epsilon_j\gamma_j; \quad T_j(6,5) = -2\epsilon_j\gamma_j; \quad T_j(6,6) = -\epsilon_j$$

$$T_j(7,3) = \eta_j\gamma_j; \quad T_j(7,7) = 1$$

$$T_j(8,2) = \eta_j^2\gamma_j^2; \quad T_j(8,3) = \eta_j(2\gamma_j^2 + \epsilon_j R_s''); \quad T_j(8,5) = 2\eta_j\gamma_j; \; T_j(8,8) = 1$$

$$T_j(9,1) = \eta_j^3\gamma_j^3; \quad T_j(9,2) = 3\eta_j^2\gamma_j(2\gamma_j^2 + \epsilon_j R_s''); \quad T_j(9,3) = \eta_j(6\gamma_j^3 + 6\epsilon_j\gamma_j R_s'' + \epsilon R_s''')$$

$$T_j(9,4) = 3\eta_j^2\gamma_j^2; \quad T_j(9,5) = 3\eta_j(\epsilon_j R_s'' + 2\gamma_j^2); \quad T_j(9,6) = 3\eta_j\gamma_j; \quad T_j(9,9) = 1. \qquad [A4]$$

All other elements are zeroes; $j$ denotes the corresponding phase and

$$R_j = (j-1)R_{\max}; \quad \epsilon_j = \frac{1}{R_j - R_s}; \quad \gamma_j = \epsilon_j R_s'; \quad R_s' = \frac{\partial R_s}{\partial z}; \quad R_s'' = \frac{\partial^2 R_s}{\partial z^2}; \quad R_s''' = \frac{\partial^3 R_s}{\partial z^3}. \qquad [A5]$$

$[T_j]$ is a $9 * 9$ lower triangular matrix. Thus, the expression of the $l$th element of $\{D^{r,z}\}$ in the new coordinates is given by

$$D^{r,z}(l) = \sum_{m=1}^{m=1} T_j(l,m) D^{\eta_j,\xi}(m). \qquad [A6]$$

In addition, the time derivative is transformed as

$$\left.\frac{\partial}{\partial t}\right)_{r,z} = \left.\frac{\partial}{\partial \tau}\right)_{\eta_j,\xi} + \eta_j\epsilon_j V_f \left.\frac{\partial}{\partial \eta_j}\right)_{\xi,\tau} \qquad [A7]$$

where

$$V_f = V_s - U_s\frac{\partial R_s}{\partial z}. \qquad [A8]$$

## APPENDIX B

*Elimination of the Pressure Term in the Normal Stress Condition*

Equation [11] gives

$$[\![P]\!] = \left[\!\!\left[ \mathrm{Oh}_1\left(\frac{\mu}{\mu_1}\right)\left[ 2\left(\frac{\partial V}{\partial r}\cos^2\alpha + \frac{\partial U}{\partial z}\sin^2\alpha\right) - \left(\frac{\partial V}{\partial z} + \frac{\partial U}{\partial r}\right)\sin 2\alpha \right]\right]\!\!\right] + \left(\frac{\cos\alpha}{R_s} - R_s''\cos^3\alpha\right). \qquad [B1]$$

Let us replace this expression by

$$[\![P]\!] = [\![PV]\!] + (PC). \qquad [B2]$$

Then noting that

$$\frac{\partial}{\partial q} = \cos\alpha\frac{\partial}{\partial \xi} \quad \text{at} \quad \eta_j = 1 \qquad [B3]$$

where $q$ is the curvilinear coordinate, the differentiation of the pressure difference [B2] along the surface gives

$$\frac{\partial [\![P]\!]}{\partial q} = \cos\alpha\frac{\partial [\![P]\!]}{\partial \xi} = \cos\alpha\left[\!\!\left[ \frac{\partial P}{\partial \xi} \right]\!\!\right] \qquad [B4]$$

with

$$\left[\!\!\left[ \frac{\partial P}{\partial \xi} \right]\!\!\right] = \left[\!\!\left[ \frac{\partial (PV)}{\partial \xi} \right]\!\!\right] + \left(\frac{\partial (PC)}{\partial \xi}\right). \qquad [B5]$$

Using the Navier–Stokes equations, one can obtain another expression of

$$\left[\!\left[ \frac{\partial P}{\partial \xi} \right]\!\right].$$

The $(U, V, P)$ nondimensional forms of the Navier–Stokes equations are

$$\frac{\rho}{\rho_1}\frac{\mathrm{D}V}{\mathrm{D}t} = -\frac{\partial P}{\partial r} + \mathrm{Oh}_1 \frac{\mu}{\mu_1}\left(\Delta V - \frac{V}{r^2}\right) \qquad [B6]$$

$$\frac{\rho}{\rho_1}\frac{\mathrm{D}U}{\mathrm{D}t} = -\frac{\partial P}{\partial z} + \mathrm{Oh}_1 \frac{\mu}{\mu_1}\Delta U \qquad [B7]$$

where

$$\Delta = \frac{\partial^2}{\partial r^2} + \frac{1}{r}\frac{\partial}{\partial r} + \frac{\partial^2}{\partial z^2}. \qquad [B8]$$

In both phases, $\rho_1 U_0^2$ has been used as a characteristic pressure.

By definition

$$\frac{\partial P}{\partial z} = \frac{\partial P}{\partial \xi} + \epsilon_j R_s' \frac{\partial P}{\partial \eta} \quad \text{at} \quad \eta_j = 1. \qquad [B9]$$

Thus

$$\frac{\partial P}{\partial \xi} = \frac{\partial P}{\partial z} + R_s' \frac{\partial P}{\partial r}. \qquad [B10]$$

Substituting in each phase $\partial P/\partial r$ and $\partial P/\partial z$ by their expressions given, respectively, by [B6] and [B7], one easily comes to the difference

$$\left[\!\left[ \frac{\partial P}{\partial \xi} \right]\!\right] = \left[\!\left[ -\frac{\rho}{\rho_1}\left(\frac{\mathrm{D}U}{\mathrm{D}t} + R_s' \frac{\mathrm{D}V}{\mathrm{D}t}\right) + \mathrm{Oh}_1\left(\frac{\mu}{\mu_1}\right)\left[ \Delta U + R_s'\left(\Delta V - \frac{V}{r^2}\right)\right]\right]\!\right]. \qquad [B11]$$

Let us write [B11] as

$$\left[\!\left[ \frac{\partial P}{\partial \xi} \right]\!\right] = [\![M]\!]. \qquad [B12]$$

We thus have

$$[\![M]\!] = \left[\!\left[ \frac{\partial (PV)}{\partial \xi} \right]\!\right] + \left(\frac{\partial (PC)}{\partial \xi}\right). \qquad [B13]$$

Equation [B13] is then transformed to [23] using relations [2] and appendix A. In this section, subscript $j$ has been omitted.

## APPENDIX C

*Coefficients in [19]–[23] and [25]*

Setting $\chi = 1/R_s$, $Z = \mathrm{Oh}_1 \nu_j/\nu_1$, $\mathrm{Oh} = \mathrm{Oh}_1 \mu_j/\mu_1$, $r = [\eta_j R_s + R_j(1 - \eta_j)]$ the coefficients are:

$$a_{1_j} = Z(\epsilon_j^2 + \eta_j^2 \gamma_j^2), \quad a_{2_j} = [Z(r^{-1}(-\epsilon_j) + \eta_j(2\gamma_j^2 + \epsilon_j R_s'')) - (\eta_j \epsilon_j V_f - \epsilon_j V_j + \eta_j \gamma_j U_j)]$$
$$a_{3_j} = 2Z\eta_j\gamma_j, \quad a_{4_j} = -U_j, \quad a_{5_j} = Z, \quad a_{6_j} = r^{-1}(V_j - r^{-1}Z) \qquad [C1]$$

$$b_{1_j} = (\eta_j^2\gamma_j^2 + \epsilon_j^2), \quad b_{2_j} = (\eta_j(2\gamma_j^2 + \epsilon_j R_s'') + \epsilon_j r^{-1}), \quad b_{3_j} = 2\eta_j\gamma_j \qquad [C2]$$

$$g_{1_j} = r^{-1}, \quad g_{2_j} = \eta_j \gamma_j r^{-1}; \quad g_{3_j} = \epsilon_j r^{-1} \qquad [C3]$$

$$c_{1_j} = \frac{\mu_j}{\mu_1}\chi(-2\epsilon_j\gamma_j \tan 2\alpha + \gamma_j^2 - \chi\epsilon_j^2), \quad c_{2_j} = \frac{\mu_j}{\mu_1}\chi[(-\chi\gamma_j - 2\epsilon_j\gamma_j)\tan 2\alpha + (2\gamma_j^2 + \epsilon_j R_s'') - \chi\epsilon_j]$$

$$c_{3_j} = 2\frac{\mu_j}{\mu_1}\chi(-\epsilon_j \tan 2\alpha + \gamma_j), \quad c_{4_j} = -\frac{\mu_j}{\mu_1}\chi^2 \tan 2\alpha, \quad c_{5_j} = \frac{\mu_j}{\mu_1}\chi \qquad [C4]$$

$$d_{1j} = -\mathrm{Oh}\chi(\epsilon_j^3 + 2\epsilon_j\gamma_j^2 + \gamma_j^3 R_s'), \quad d_{2_j} = -\mathrm{Oh}\chi[6\gamma_j^2(\epsilon_j + \gamma_j R_s') + R_s''(3\gamma_j^2 + \epsilon_j^2) + \chi(\gamma_j^2 + \epsilon_j^2)]$$

$$d_{3_j} = \mathrm{Oh}\epsilon_j\chi[2\epsilon_j R_s'^2(\chi - 2\epsilon_j) + R_s''^2(-2\cos^2\alpha\cos 2\alpha) - R_s''' \sin 2\alpha - 2R_s''(\epsilon_j + \sin^2\alpha(\epsilon_j - \chi))]$$

$$-\mathrm{Oh}\chi[\epsilon_j(\chi^2 + 2\gamma_j^2 + \epsilon_j R_s'') + \gamma_j^2\chi + \gamma_j(6\gamma_j^2 R_s' + 6\gamma_j R_s'' + R_s''')]$$

$$+\chi\frac{\rho_j}{\rho_1}\left[(1 + R_s'^2)\left(\frac{\epsilon_j}{\Delta\tau} + U_s\chi R_s'\right) + U_s R_s'(\epsilon_j + \gamma_j R_s' + R_s'')\right]$$

$$d_{4_j} = -3\mathrm{Oh}\chi\epsilon_j\gamma_j(1 + R_s'^2)$$

$$d_{5_j} = 2\mathrm{Oh}\chi\gamma_j(\chi - 2\epsilon_j - R_s''\cos^2\alpha) - \chi\left[\mathrm{Oh}\gamma_j(2\epsilon_j + \chi + 6\gamma_j R_s' + 3R_s'') - \frac{\rho_j}{\rho_1}U_s\epsilon_j(1 + R_s'^2)\right]$$

$$d_{6_j} = -3\mathrm{Oh}\chi\epsilon_j(1 + R_s'^2), \quad d_{7_j} = 2\mathrm{Oh}\chi^2 \sin 2\alpha(\chi + R_s''\cos^2\alpha) + \chi R_s'\frac{\rho_j}{\rho_1}\left(\frac{1}{\Delta\tau} - \chi U_s R_s'\right)$$

$$d_{8_j} = -2\mathrm{Oh}\chi\cos 2\alpha(\chi + R_s''\cos^2\alpha) + \chi U_s R_s'\frac{\rho_j}{\rho_1}, \quad d_{9_j} = -\mathrm{Oh}\chi(\sin 2\alpha + R_s')$$

$$s = [\chi \sin\alpha(\chi + \cos^2\alpha R_s'') + \cos^3\alpha R_s''' - 3\sin\alpha\cos^4\alpha R_s''^2] + \frac{1}{\Delta\tau}\left(1 - \frac{\rho_2}{\rho_1}\right)(U_s^n + R_s' V_s^n) \qquad [C5]$$

where $n$ denotes the previous time step, $\epsilon_j$, $\gamma_j$, ... are defined in appendix A.

$$b_w = [R_{\max}(R_{\max} - R_s)^2]^{-1}. \qquad [C6]$$

## APPENDIX D

*List of the Characteric Parameters of Different Liquid–Liquid Systems Involved in this Paper*

| Systems no. | Systems Inner liquid (1)–Outer fluid (2) | Density $\rho_1$ (g/cm$^3$) | Density $\rho_2$ (g/cm$^3$) | Viscosity $\mu_1$ (poises) | Viscosity $\mu_2$ (poises) | Surface tension $\sigma_{12}$ (dyne/cm) |
|---|---|---|---|---|---|---|
| | Water–gas | 1.0 | 0.0 | 0.01 | 0.0 | 72.5 |
| | Water–Dodecan | 1.0 | 0.748 | 0.01 | 0.0135 | 47 |
| | Liquid 1–gas | 1.0 | 0.0 | 0.01 | 0.0 | 47 |
| | Liquid 1–Liquid 2 | 1.0 | 0.374 | 0.01 | 0.0135 | 47 |
| | Liquid 1–Liquid 1 | 1.0 | 1.0 | 0.01 | 0.01 | 50 |
| | Liquid 3–Liquid 1 | 10.0 | 1.0 | 0.01 | 0.01 | 50 |
| 1–1† | *n*-Heptane–water | 0.676 | 0.996 | 0.00403 | 0.00829 | 51.2 |
| 3–2† | Kerosene + liquid paraffin–water | 0.848 | 0.998 | 0.188 | 0.0103 | 40.2 |
| 4–1† | *n*-Heptane–aq. sol. of starch syrup | 0.683 | 1.126 | 0.00407 | 0.0371 | 56 |
| 6–1† | Kerosene + liquid paraffin–aq. sol. of Starch syrup | 0.831 | 1.117 | 0.08 | 0.0278 | 43 |
| A‡ | Silicone oil 1000–Castor oil | 0.973 | 0.959 | 10.7 | 7.28 | 5.2 |
| B‡ | Silicone oil 100–Castor oil | 0.968 | 0.959 | 1.08 | 7.28 | 4.6 |

†The systems of this numeration are drawn from the paper of Kitamura *et al.* (1982).
‡The systems of these symbols are from the paper of Mikami and Mason (1975).